To appear in ApJ

The Isophotal Structure of Early-Type Galaxies in the SDSS: Dependence on AGN Activity and Environment.

Anna Pasquali, Frank C. van den Bosch and Hans-Walter Rix

Max-Planck-Institut für Astronomie, Königstuhl 17, D-69117 Heidelberg, Germany

pasquali@mpia.de, vdbosch@mpia.de, rix@mpia.de

ABSTRACT

We study the dependence of the isophotal shape of early-type galaxies on their absolute B-band magnitude, M_B, their dynamical mass, $M_{\rm dyn}$, and their nuclear activity and environment, using an unprecedented large sample of 847 early-type galaxies identified in SDSS by Hao et al. (2006a). We find that the fraction of disky galaxies smoothly decreases from $f_{\rm disky} \sim 0.8$ at $M_B - 5\log(h) = -18.7$ ($M_{\rm dyn} = 6 \times 10^{10} h^{-1} M_\odot$) to ~ 0.5 at $M_B - 5\log(h) = -20.8$ ($M_{\rm dyn} = 3 \times 10^{11} h^{-1} M_\odot$). The large sample allows us to describe these trends accurately with tight linear relations that are statistically robust against the uncertainty in the isophotal shape measurements. There is also a host of significant correlations between $f_{\rm disky}$ and indicators of nuclear activity (both in the optical and in the radio) and environment (soft X-rays, group mass, group hierarchy). Our analysis shows however that these correlations can be accurately matched by assuming that $f_{\rm disky}$ *only* depends on galaxy luminosity or mass. We therefore conclude that neither the level of activity, nor group mass or group hierarchy help in better predicting the isophotal shape of early-type galaxies.

Subject headings: galaxies: active — galaxies: elliptical and lenticular, cD — galaxies: Seyfert — galaxies: structure

1. Introduction

Early-type galaxies form a remarkably homogeneous class of objects with a well-defined Fundamental Plane and with tight relations between colour and magnitude, between colour and velocity dispersion, and between the amount of α-element enhancement and velocity dispersion (e.g., Faber & Jackson 1976; Visvanathan & Sandage 1977; Dressler 1987; Djorgovski & Davis 1987; Bower et al. 1992; Ellis et al. 1997). They have old stellar populations, though sometimes with a younger component (Trager et al. 2000; Serra et al. 2006; Kuntschner et al. 2006), contain little ionized and cold gas (Sarzi et al. 2006; Morganti et al. 2006), and are preferentially located in massive dark matter halos (e.g., Dressler 1980; Weinmann et al. 2006).

Ever since the seminal work by Davies et al. (1983), however, it has become clear that early-type galaxies encompasses two distinct families. Davies et al. showed that bright ellipticals typically have little rotation, such that their flattening must originate from anisotropic pressure. This is consistent with bright ellipticals being in general triaxial. Low luminosity ellipticals, on the other hand, typically have rotation velocities that are consistent with them being oblate isotropic rotators. With the advent of CCD detectors, it quickly became clear that these different kinematic classes also have different morphologies. Although ellipticals have isophotes that are ellipses to high accuracy, there are small deviations from perfect ellipses (e.g., Lauer 1985; Carter 1987; Bender & Möllenhoff 1987). In particular, bright, pressure-supported systems typically have boxy isophotes, while the lower luminosity, rotation-supported systems often reveal disky isophotes (e.g., Bender 1988; Nieto et al. 1988). With the high angular resolution of the Hubble Space Telescope it has become clear that both types have different central surface brightness profiles as well. The bright, boxy ellipticals typically have luminosity profiles that break from steep outer power-laws to shallow inner cusps (often called 'cores'). The fainter, disky ellipticals, on the other hand, have luminosity profiles that lack a clear break and have a steep central cusp (e.g., Jaffe et al. 1994; Ferrarese et al. 1994; Lauer et al. 1995; Gebhardt et al. 1996; Faber et al. 1997; Rest et al. 2001; Ravindranath et al. 2001; Lauer et al. 2005).

The isophotal shapes of early-type galaxies have also been found to correlate with the radio and X-ray properties of elliptical galaxies (Bender et al. 1989; Pellegrini 1999). Objects which are radio-loud and/or bright in soft X-ray emission generally have boxy isophotes, while disky ellipticals are mostly radio-quiet and faint in soft X-rays. As shown in Pellegrini (2005), the soft X-ray emission of power-law (and hence disky) ellipticals is consistent with originating from X-ray binaries. Ellipticals with a central core (which are mainly boxy), however, often have soft X-ray emission in excess of what may be expected from X-ray binaries. This emission originates from a corona of hot gas which is distributed beyond the optical radius of the galaxy (e.g., Trinchieri & Fabbiano 1985, Canizares et al. 1987; Fabbiano 1989). In terms of the radio and hard X-ray emission, thought to originate from active galactic nuclei (AGN), it is found that those ellipticals with the highest luminosities in radio and/or hard X-rays are virtually always boxy (Bender et al. 1989; Pellegrini 2005). This is consistent with the results of Ravindranath et al. (2001), Lauer et al. (2005) and Pellegrini (2005), all of whom find a somewhat higher fraction of ellipticals with optical AGN activity (i.e., nuclear line emission) among cored galaxies.

The above mentioned trends between isophotal shape and galaxy properties have mainly been based on relatively small, somewhat heterogenious samples of relatively few objects ($\lesssim 100$). Recently, however, Hao et al. (2006a, hereafter H06) compiled a sample of 847 nearby, early-type galaxies from the Sloan Digital Sky Survey (SDSS) for which they measured the isophotal shapes. Largely in agreement with the aforementioned studies they find that (i) more luminous galaxies are on average rounder and are more likely to have boxy isophotes (ii) disky ellipticals favor field environments, while boxy ellipticals prefer denser environments, and (iii) disky ellipticals tend to lack powerful radio emission, although this latter trend is weak.

The prevailing idea as to the origin of this disky-boxy dichotomy is that it reflects the galaxy's assembly history. Within the standard, hierarchical formation picture, in which ellipticals are formed via mergers, the two main parameters that determine whether an elliptical will be boxy and cored or disky and cuspy are the progenitor mass ratio and the progenitor gas mass fractions. Pure N-body simulations without gas show that the isophotal shapes of merger remnants depend sensitively on the progenitor mass ratio: major mergers create ellipticals with boxy isophotes, while minor mergers mainly result in systems with disky isophotes (Khochfar & Burkert 2005, Jesseit et al. 2005). As shown by Naab et al. (2006), including even modest amounts of gas has a dramatic impact on the isophotal shape of equal-mass merger remnants. The gas causes a significant reduction of the fraction of box and boxlet orbits with respect to collisionless mergers, and the remnant appears disky rather than boxy. Therefore, it seems that the massive, boxy ellipticals can only be produced via dry, major mergers. The cores in these boxy ellipticals are thought to arise from the binding energy liberated by the coalescence of supermassive binary black holes during the major merger event (e.g., Faber et al. 1997; Graham et al. 2001; Milosavljević et al. 2002). When sufficient gas is present, however, dissipation and sub-sequent star formation may regenerate a central cusp. Alternatively, the gas may serve as an energy sink for the binding energy of the black hole binary, leaving the original stellar cusp largely intact. Thus, following Lauer et al. (2005), we may summarize this picture as implying that power-laws reflect the outcome of dissipation and concentration, while cores owe to mixing and scattering.

But what about the correlation between isophotal shape and AGN activity? It is tempting to believe that this correlation simply derives from the fact that both isophotal shape and AGN activity may be related to mergers. After all, it is well known that mergers can drive nuclear inflows of gas, which produce starbursts and feed the central supermassive black hole(s) (Toomre & Toomre 1972, Barnes & Hernquist 1991,1996, Mihos & Hernquist 1994,1996, Springel 2000, Cattaneo et al. 2005). However, since the onset of such AGN activity requires wet mergers, this would predict a higher frequency of AGN among disky ellipticals, contrary to the observed trend. Another argument against mergers being responsible for the AGN-boxiness correlation is that the time scale for merger-induced AGN activity is relatively short ($\lesssim 10^8$ yrs) compared to the dynamical time in the outer parts of the merger remnant. This implies that active ellipticals should reveal strongly distorted isophotes, which is not the case.

An important hint may come from the strong correlation between the presence of dust (either clumpy, filamentary, or in well defined rings and disks) and the presence of optical emission line activity (Tran et al. 2001; Ravindranath et al. 2001; Lauer et al. 2005). Although this suggests that this dust is (related to) the actual fuel for the AGN activity, many questions remain. For instance, it is unclear whether the origin of the dust is internal (shed by stellar winds) or external (see Lauer et al. 2005 for a detailed discussion). In addition, it is not clear why the presence of dust, and hence the AGN activity, would be more prevalent in boxy ellipticals. One option is that boxy ellipticals are preferentially central galaxies (as opposed to satellites), so that they are more efficient at accreting external gas (and dust). This is consistent with the fact that boxy ellipticals (i) are, on

average, brighter, (ii) reside in dense environments (Shioya & Taniguchi 1993; H06), and (iii) more often contain hot, soft X-ray emitting halos. Another, more benign possibility, is that the relation between morphology and AGN activity is merely a reflection of the fact that both morphology and AGN activity depend on the magnitude of the galaxy (or on its stellar or dynamical mass). In this case, AGN activity is only indirectly related to the morphology of its host galaxy.

In this paper we use the large data set of H06 to re-investigate the correlations between morphology and (i) luminosity, (ii) dynamical mass, and (iii) emission line activity in the optical, where we discriminate between AGN activity and star formation. In addition, we also examine to what extent morphology correlates with X-ray emission (using data from ROSAT), with 1.4GHz radio emission (using data from FIRST), and with the mass of the dark matter halo in which the galaxy resides (using a SDSS galaxy group catalog). The outline of this paper is as follows. In § 2 we describe the data of H06; in § 3 we present the fraction of disky galaxies across the full sample as a function of galaxy luminosity, dynamical mass and environment. In § 4 we split the sample galaxies according to their activity in the optical, radio and X-rays, and investigate how the disky-boxy morphology correlates with these various levels of 'activity'. Finally, in § 5 we summarize and discuss our findings. Throughout this paper we adopt a ΛCDM cosmology with $\Omega_m = 0.3$, $\Omega_\Lambda = 0.7$, and $H_0 = 100h\,\mathrm{km\,s^{-1}\,Mpc^{-1}}$. Magnitudes are given in the AB system.

2. Data

2.1. Sample Selection

In order to investigate the interplay among AGN activity, morphology and environment for early-type galaxies, we have analyzed the sample of H06, which consists of 847 galaxies in the SDSS DR4 (Adelman-McCarthy et al. 2006) classified as ellipticals (E) or lenticulars (S0). As described in H06, these objects are selected to be at $z < 0.05$, in order to ensure sufficient spatial resolution to allow for a meaningful measurement of the isophotal parameters. In addition, the galaxies are selected to have an observed velocity dispersion between $200\,\mathrm{km\,s^{-1}}$ and $420\,\mathrm{km\,s^{-1}}$ (where the upper limit corresponds to the largest velocity dispersion that can be reliably measured from the SDSS spectra), and are not allowed to be saturated. Note that, for the median sample distance, the fiber radius of 1.5 arcsec corresponds to about 30% of the sample mean effective radius. From all galaxies that obey these criteria, early-types have been selected by H06 using visual inspection. Galaxies with prominent dust lanes have been excluded from the final sample in order to reduce the effects of dust on the isophotal analysis.

2.2. Isophotal Analysis

Isophotes are typically parameterized by their corresponding surface brightness, I_0, their semi-major axis length, a, their ellipticity, ϵ, and their major axis position angle, θ_0. In addition, since isophotes are not perfectly elliptical, it is common practice to expand the angular intensity variation along the best fit ellipse, $\delta I(\theta)$, in a Fourier series:

$$\delta I(\theta) = \sum_{n=3}^{n=4} \left[A'_n \cos n(\theta - \theta_0) + B'_n \sin n(\theta - \theta_0) \right] \tag{1}$$

(e.g., Carter 1987; Jedrzejewski 1987; Bender & Möllenhoff 1987). Only the terms with $n = 3$ and $n = 4$ are usually computed, as the data is often too noisy to reliably measure higher-order terms (but see Scorza & Bender 1995 and Scorza & van den Bosch 1999). Note that, by definition, the terms with $n = 0$, 1, and 2 are equal to zero within the errors. If the isophote is perfectly elliptical, then A'_n and B'_n are also equal to zero for $n \geq 3$. Non-zero A'_3 and B'_3 express deviations from a pure ellipse that occur along the observed isophote every 120°. Typically, such deviations arise from the presence of dust features or clumps. The most important Fourier coefficient, however, is A'_4, which quantifies the deviations taking place along the major and minor axes. Isophotes with $A'_4 < 0$ have a 'boxy' shape, while those with a positive A'_4 parameter are 'disk'-shaped.

For each of the 847 E/S0 galaxies in their sample H06 measured the isophotal parameters using the `IRAF`[1] task `ELLIPSE`. In particular, for each galaxy they provide the ellipticity, ϵ, the position angle of the major axis, θ_0, and the third and fourth order Fourier coefficients A_3 and A_4, which are equal to A'_3 and A'_4, respectively, divided by the semi-major axis length and the local intensity gradient. All the available parameters are intensity-weighted averages over the radial interval $2R_s < R < 1.5R_{50}$. Here R_s is the seeing radius (typically lower than 1.5 arcsec, Stoughton et al. 2002) and R_{50} is the Petrosian half-light radius[2]. The Petrosian radius is defined as the radius at which the ratio of the local surface brightness to the mean interior surface brightness is 0.2 (cf. Strauss et al. 2002). Therefore, R_{50} is the radius enclosing half of the flux measured within a Petrosian radius and can be used as a proxy for the galaxy effective radius R_e. In what follows, we refer to galaxies with $A_4 \leq 0$ and $A_4 > 0$ as 'boxy' and 'disky', respectively.

In their seminal papers on the isophotal shapes of elliptical galaxies, Bender & Möllenhoff (1987), Bender et al. (1988) and Bender et al. (1989) define alternative structural parameters, a_n/a and b_n/a, which are related to the A_n and B_n parameters defined here as

$$\frac{a_n}{a} = \sqrt{1-\epsilon}\, A_n \qquad \frac{b_n}{a} = \sqrt{1-\epsilon}\, B_n \tag{2}$$

(Bender et al. 1988; Hao et al. 2006b).

[1] `IRAF` is distributed by the National Optical Astronomy Observatories, which are operated by the Asssociation of Universities for Research in Astronomy, Inc., under cooperative agreement with the National Science Foundation

[2] These data are publicly available at http://www.jb.man.ac.uk∼smao/isophote.html

2.3. Additional data

For all galaxies in the H06 sample we determined the absolute magnitudes in the SDSS g, r and i bands, corrected for Galactic extinction, and K-corrected to $z = 0$, using the luminosity distances corrected for Virgo-centric infall of the Local Group (LG) following Blanton et al. (2005). In order to allow for a comparison with the samples of Bender et al. (1989) and Pellegrini (1999, 2005), we transform these magnitudes to those in the Johnson B-band using the filter transformations given by Smith et al. (2002).

We also estimated, for each galaxy, the total dynamical mass as

$$M_{\rm dyn} = A\frac{\sigma^2_{\rm corr}R_{50}}{G} \tag{3}$$

Here G is the gravitational constant, A is a normalization constant, and $\sigma_{\rm corr}$ is the velocity dispersion measured from the SDSS spectra corrected for aperture effects using

$$\sigma_{\rm corr} = \sigma_{\rm measured}\left(\frac{R_{\rm fiber}}{R_{50}/8}\right)^{0.04}, \tag{4}$$

with $R_{\rm fiber} = 1.5$ arcsec (Bernardi et al. 2003). The aperture correction is meant to give the velocity dispersion within $R_{50}/8$, and to make comparable galaxies at different distance but sampled with a spectroscopic fiber of fixed size. Throughout this paper we adopt $A = 5$, which has been shown to accurately reproduce the total dynamical masses inferred from more accurate modeling (Cappellari et al. 2006[3]). Note that Cappellari et al. have also shown that these dynamical masses are roughly proportional to the stellar masses of early-type galaxies.

H06 cross-correlated their E/S0 sample with the FIRST radio survey (Becker, White & Helfand 1995), which yielded the 1.4GHz fluxes for 162 objects in the sample. In order to investigate the relation between isophotal structure and soft X-ray properties, we also matched the H06 sample to the ROSAT All Sky Survey Catalog (Voges et al. 1999). This yields ROSAT/PSPC count-rates in the 0.1 – 2.4 keV energy band for 40 sample galaxies. We used the WebPIMMS tool[4] to transform the observed count-rates into astrophysical fluxes, corrected for Galactic extinction, assuming an X-ray power-law spectrum with energy index $\alpha_X = 1.5$ (cf. Anderson et al. 2003). In addition, we cross-identified the H06 sample with the spectroscopic catalogs released for DR4 by Kauffmann et al. (2003a,b), and extracted, when available, the luminosity of the [OIII] λ5007 line corrected for dust extinction (in ergs^{-1}), the line-flux ratios [OIII]/Hβ and [NII]/Hα, and the S/N values associated with the [OIII] and Hα fluxes.

---

[3]Cappellari et al. (2006) use a slightly different definition of $\sigma_{\rm corr}$ in equation (2), namely that measured within R_e rather than $R_{50}/8$. Given the weak dependence of the velocity dispersion on the enclosed radius, we estimate that this difference results in an offset of $\sim$0.07 dex in $M_{\rm dyn}$

[4]http://heasarc.gsfc.nasa.gov/Tools/w3pimms.html

Finally, in order to assess the environment of the sample galaxies, we cross-identified the H06 sample with the SDSS group catalog of Weinmann et al. (2006; hereafter WBYM), which is constructed using the halo-based group finder of Yang et al. (2005). This yields group (i.e. dark matter halo) masses for a total of 431 galaxies, distributed over 403 groups. Of these, 350 are 'central' galaxies (defined as the brightest galaxy in its group) and 81 are 'satellites'. As for the groups, 83 have just a single member (the early-type galaxy in our sample), while 320 groups have 2 or more members. The fact that only 51 percent of the galaxies in the H06 sample are affiliated with a group is due to the fact that the WBYM group catalog is based on the DR2, and to the fact that not all galaxies can be assigned to a group (see Yang et al. 2005 for details).

3. The disky fraction across the sample

The main properties of the full H06 sample (comprising all 847 early-type galaxies) are summarized in Figure 1. The sample spans about 3 orders of magnitude in M_B ($-17.8 > M_B - 5\log(h) > -21.4$) and a range of about 1.5 dex in dynamical mass ($10.5 < \log[M_{\rm dyn}(h^{-1}M_\odot)] < 12$) and 3 dex in group (halo) mass ($11.8 < \log[M_{\rm group}(h^{-1}M_\odot)] < 15$). As expected, the B-band magnitude is well correlated with the dynamical mass, independent of whether the galaxy is a central galaxy or a satellite, and independent of whether it is disky or boxy. The absolute magnitudes and dynamical masses of satellite galaxies are clearly separated from those of the central galaxies when plotted as function of the group (halo) mass. This simply reflects that centrals are defined as the brightest (and, hence, most likely the most massive) group members. This clear segregation disappears when the galaxies are split in disky and boxy systems (lower panels), indicating that there is no strong correlation between morphology and group hierarchy.

The upper panels of Figure 2 show scatter plots of M_B, $M_{\rm dyn}$ and $M_{\rm group}$ as function of the isophotal parameter A_4. They indicate that the fraction of disky systems (those with $A_4 > 0$) increases with decreasing luminosity and dynamical mass, in qualitative agreement with Bender et al. (1989) and H06. In the case of $M_{\rm group}$, a similar trend seems to be present, but only for the central galaxies. In order to quantify these trends, we have computed the fraction, $f_{\rm disky}$, of disky galaxies as a function of M_B, $M_{\rm dyn}$ and $M_{\rm group}$. For each bin in absolute magnitude, dynamical mass, or group mass, $f_{\rm disky}$ is defined as the number ratio between disky galaxies and the total number of galaxies in that bin. Each bin contains at least ten disky galaxies. For comparison, the disky fraction of the full H06 sample is 0.66.

The lower left-hand panel of Figure 2 plots $f_{\rm disky}$ as function of M_B. The errorbars are computed assuming Poisson statistics. The fraction of disky galaxies declines by a factor of about 1.6 from ~ 0.8 at $M_B - 5\log(h) = -18.7$ to ~ 0.5 at $M_B - 5\log(h) = -20.8$, and is well fitted by

$$f_{\rm disky}(M_B) = (0.61 \pm 0.02) + (0.17 \pm 0.03)\,[M_B - 5\log(h) + 20] \qquad (5)$$

which is shown as the solid, grey line. Note that this relation should not be extrapolated to arbitrary faint and/or bright magnitudes. Since $0 \leq f_{\rm disky} \leq 1$ it is clear that $f_{\rm disky}(M_B)$ must flatten at

both ends of the magnitude distribution. Apparently the magnitude range covered by our sample roughly corresponds to the range in which the distribution transits (relatively slowly and smoothly) from mainly disky to mainly boxy.

It has to be noted that the exact relation between $f_{\rm disky}$ and M_B is somewhat sensitive to the exact sample selection criteria, and equation (5) therefore has to be used with some care.

We have tested the robustness of the above relation by adding Gaussian deviates to each measured value of A_4, and then recomputing the best-fit relation between $f_{\rm disky}$ and M_B. Figure 3 shows the slope and zero-point of this relation as function of the standard deviation of the Gaussian deviates used (filled circles). The grey shaded horizontal bar represents the 1 σ interval around the best-fit slope (left-hand panel) and the best-fit zero-point (right-hand panel). The grey shaded vertical bar indicates the mean uncertainty on the observed A_4 parameter obtained by H06 ($\sigma(A_4) = 0.0012 \pm 0.0008$). Note that the best-fit slope and zero-point are extremely robust. Adding an artificial error to the A_4 measurements with an amplitude that is a factor five larger than the average error quoted by H06 yields best-fit values that agree with those of equation (5) at better than the 1σ errorbar on these parameters obtained from the fit.

The middle panel in the lower row of Figure 2 plots $f_{\rm disky}$ as function of $M_{\rm dyn}$. As with the luminosity, the disky fraction decreases smoothly with increasing dynamical mass, dropping from ~ 0.80 at $M_{\rm dyn} = 6 \times 10^{10} h^{-1}\,{\rm M}_\odot$ to ~ 0.45 at $M_{\rm dyn} = 3 \times 10^{11} h^{-1}\,{\rm M}_\odot$. The grey, dashed line indicates the best-fit log-linear relation, which is given by

$$f_{\rm disky}(M_{\rm dyn}) = (0.73 \pm 0.02) - (0.53 \pm 0.08) \log \left[\frac{M_{\rm dyn}}{10^{11} h^{-1}\,{\rm M}_\odot} \right] \qquad (6)$$

As for equation (5), the Gaussian-deviates test shows that this relation is robust against uncertainties in the A_4 measurements.

As is well-known from the morphology-density relation (e.g., Dressler 1980), early-type galaxies preferentially reside in denser environments and hence in more massive halos (e.g, Croton et al. 2005; Weinmann et al. 2006). It is interesting to investigate whether the halo mass also determines whether the early-type galaxies are disky or boxy. We can address this using the WBYM group catalog described in §2.3. The lower right-hand panel of Figure 2 plots the disky fraction of centrals (crosses) and satellites (open triangles) as function of group mass. The fraction of disky centrals decreases with increasing group (halo) mass, declining from ~ 0.82 at $M_{\rm group} = 1.7 \times 10^{12} h^{-1}\,{\rm M}_\odot$ to ~ 0.54 at $M_{\rm group} = 5.0 \times 10^{13} h^{-1}\,{\rm M}_\odot$. For the most massive groups, we have enough satellite galaxies to also compute their disky fraction. Interestingly, these are larger (though only marginally so) than those of central galaxies in groups of the same mass.

Although these results seem to suggest that group mass and group hierarchy (i.e., central *vs.* satellite) play a role in determining the morphology of an early-type galaxy, they may also simply be reflections of the fact that (i) satellite galaxies are fainter than central galaxies in the same parent halo, (ii) fainter centrals typically reside in lower mass halos (cf. Figure 1), and (iii) fainter galaxies have a larger $f_{\rm disky}$. In order to discriminate between these options we proceed as follows.

Under the null-hypothesis that the isophotal structure of an early-type galaxy is only governed by the galaxy's absolute magnitude or dynamical mass, the *predicted* fraction of disky systems for a given sub-sample is simply

$$f_{\rm disky,0} = \frac{1}{N} \sum_{i=1}^{N} f_{\rm disky}(X_i) \tag{7}$$

where X_i is either $M_B - 5\log(h)$ or $\log(M_{\rm dyn})$ of the $i^{\rm th}$ galaxy in the sample, and $f_{\rm disky}(X)$ is the average relation between $f_{\rm disk}$ and X. The grey solid and dashed lines in the lower right-hand panel of Figure 2 show the $f_{\rm disky,0}(M_{\rm group})$ thus obtained, using equations (4) and (5), respectively. These are perfectly consistent with the observed trends (for both the centrals and the satellites). A possible exception is the disky fraction of central galaxies in groups with $M_{\rm group} < 3.0 \times 10^{12} h^{-1}\,{\rm M}_\odot$, which is $\sim 2.5\sigma$ higher than predicted by the null-hypothesis. Overall, however, these results support the null-hypothesis that the morphology of an early-type galaxy depends only on its luminosity or dynamical mass: there is no significant indication that group mass and/or group hierarchy have a direct impact on the morphology of early-type galaxies.

4. The disky fraction of active early-type galaxies

4.1. Defining different activity classes

In the standard unified model, AGN are distinguished in AGN of Type I when the central black hole, its continuum emission and its broad emission-line region are viewed directly, and Type II, if the central engine is obscured by a dusty circumnuclear medium. Our sample of early-type galaxies does not contain any Type I AGN, simply because these systems are not part of the main galaxy sample in the SDSS. However, the E/S0 sample of H06 is not biased against Type II AGN. In order to identify these systems, one needs to be able to distinguish them from early-types with some ongoing, or very recent, star formation, which also produces narrow emission lines. Since stars and AGN produce different ionization spectra, one can discriminate between them by using line-flux ratios. In particular, star formation and AGN activity can be fairly easily distinguished using the so-called BPT diagram (after Baldwin, Phillips & Terlevich 1981; see also Veilleux & Osterbrock 1987), whose most common version involves the line-flux ratios [OIII]/Hβ and [NII]/Hα.

Figure 4 plots the BPT diagram for those sample galaxies whose [OIII] λ5007 and Hα lines have been detected with a signal-to-noise ratio S/N ≥ 3. The solid curve was derived by Kauffmann et al. (2003b) and separates star-forming galaxies from type II AGN, with the latter lying above the curve. We follow Kauffmann et al. (2003b) and split the Type II AGN into Seyferts, LINERS, and Transition Objects (TOs) according to their line-flux ratios: Type II Seyferts have $\log([{\rm OIII}]/{\rm H}\alpha) \geq 0.5$ and $\log([{\rm NII}]/{\rm H}\alpha) \geq -0.2$, LINERS have $\log([{\rm OIII}]/{\rm H}\alpha) < 0.5$ and $\log([{\rm NII}]/{\rm H}\alpha) \geq -0.2$, and all galaxies with $\log([{\rm NII}]/{\rm H}\alpha) < -0.2$ and laying above the curve are labelled TO. Kewley et al. (2006) have recently studied in detail the properties of LINERs and type II Seyferts, and found that LINERs and Seyferts form a continuous progression in the accretion rate $\frac{L}{L_{\rm Edd}}$, with LINERs

dominating at low $\frac{L}{L_{\rm Edd}}$ and Seyferts prevailing at high $\frac{L}{L_{\rm Edd}}$. The results obtained by Kewley et al. suggest that most LINERs are AGN and require a harder ionizing radiation field together with a lower ionization parameter than Seyferts.

In order to increase the statistics of our subsequent analysis, we have organized the 847 galaxies in the H06 sample into 3 categories:

1. **AGN**: This class consists of 28 early-type galaxies with a Seyfert-like activity and 286 early-type galaxies with a LINER-like activity.

2. **Emission-line (EL)**: This class consists of those galaxies that according to the BPT diagram are star formers or transition objects, as well as those galaxies that lack one or both of the BPT line-flux ratios, but that have an [OIII] emission line with a S/N $\geq$ 3. There are a total of 383 early-type galaxies in the H06 sample that fall in this category.

3. **Non-active (NA)**: These are the 150 galaxies that are not in the AGN or EL categories. Therefore, these galaxies either have no emission lines at all, or have a detected [OIII] line but with a S/N $<$ 3. Among these, 43 objects (29 percent) show Hα emission with a S/N $\geq$ 3. Their presence could signal a problem with the spectroscopic pipeline, which failed to properly measure the [OIII] line, or be real and due to an episode of star formation in its early phases. In any case, their low S/N in [OIII] prevents us from classifying these galaxies in one of the above two categories.

Given our aim to establish the presence/absence of a correlation between the AGN activity and the disky/boxy morphology of the host early-type galaxy, the classification above is clearly driven by the detection of the [OIII] line emission, which is commonly used as a proxy for the AGN strength (cf. Kauffmann et al. 2003b, Kewley et al. 2006).

Along with these 3 categories which describe the galaxy activity in the optical, we have also defined two additional activity classes: 'FIRST', which consists of the 162 sample galaxies with a 1.4GHz flux in the FIRST catalog (Becker et al. 1995), and 'ROSAT', containing the 40 sample galaxies that have been detected in the ROSAT All Sky Survey (Voges et al. 1999). The soft X-ray luminosities of these ROSAT galaxies span the range $41.3 < \log[L_X/(\mathrm{ergs}^{-1})] < 42.7$ and are consistent (though with large scatter), with the well known $L_X \propto L_B^2$ relation (Trinchieri & Fabbiano 1985; Canizares et al. 1987). This X-ray emission is therefore associated with a hot corona surrounding the galaxy, rather than with X-ray binaries, and we can use it to indirectly probe the environment where galaxies live. As shown by Bender et al. (1989) and O'Sullivan et al. (2001), the $L_X \propto L_B^2$ relation applies to X-ray luminosities between 10^{40} and 10^{43} erg s^{-1}. Our ROSAT category is thus somehow incomplete at $40 < \log[L_X/(\mathrm{ergs}^{-1})] < 41$ and the trends discussed below for this class should be taken with some caution.

Table 1 lists the number of galaxies in each of these five activity classes. Note that the AGN, EL and NA classes are mutually exclusive, but that a galaxy in each of these three classes can

appear also in the FIRST and ROSAT sub-samples. The vast majority of the galaxies detected by FIRST or ROSAT reveal activity also in the optical, and are classified as either AGN or EL. The radio and soft X-ray detections themselves, however, are not well correlated: only 12 percent of the galaxies detected by FIRST have also been detected in soft X-rays.

Before computing $f_{\rm disky}$ for the galaxies in these various activity classes, it is useful to examine how their respective distributions in M_B, $M_{\rm group}$ and L[OIII] compare. This is shown in Figures 5, 6 and 7, respectively. While the luminosity distributions of the AGN and EL galaxies are in good agreement with that of the full sample, the galaxies detected by ROSAT are on average about half a magnitude brighter than the galaxies in the full sample. Also the non-active and radio galaxies are brighter than average, though the differences are less pronounced. McMahon et al. (2002) estimated a limiting magnitude of $R \simeq 20$ for the optical counterparts of FIRST sources at a 97 percent completeness level. Since the apparent magnitude limit of the H06 sample is brighter than this limit, the FIRST subsample extracted from H06 is to be considered complete. Therefore, the shift towards higher luminosities for the galaxies detected by FIRST with respect to the full sample in Figure 5 is real rather than an artifact due to the depth of the different surveys.

Similar trends are present with respect to the group masses: whereas AGN and EL galaxies have group masses that are very similar to those of the full sample, galaxies detected by ROSAT and FIRST seem to prefer more massive groups. Somewhat surprisingly, the same applies to the class of non-active galaxies. As for the luminosity of their [OIII] line plotted in Figure 7, AGN galaxies tend to be brighter than EL and ROSAT galaxies, while the [OIII] luminosities of FIRST galaxies are consistent with those of the EL and AGN galaxies combined (grey shaded histogram). In agreement with Best et al. (2005), no correlation is found between the radio and [OIII] luminosities of the sample galaxies in common with FIRST. Finally, it is worth emphasizing that the optical activity defined in this paper occurs at $\log(L_{\rm [OIII]}/L_\odot) \geq 4.6$; therefore, the class of non-active galaxies may also contain weak AGN with [OIII] fluxes below this limit. Using the KS-test, we have investigated whether the various distributions are consistent with being drawn from the same parent distribution. We have found that only EL and ROSAT are consistent, in terms of their [OIII] luminosity, with belonging to the same population, as well as the pairs (AGN,EL) and (NA,FIRST) in terms of their absolute magnitude, the pair (AGN,EL) with respect to their dynamical mass, and the pairs (AGN,EL), (NA,FIRST), (NA,ROSAT) and (FIRST,ROSAT) in terms of their group halo mass.

Another aspect of defining different modes of activity is to study their actual frequency, i.e. the fraction of galaxies sharing the same kind of activity (with respect to the full sample) as a function of M_B, $M_{\rm dyn}$ and environment. This is plotted in Figure 8, where the percentage of NA, FIRST and ROSAT galaxies increases by a factor of about 4 towards higher luminosities and larger dynamical masses (cf. Best et al. 2005, O'Sullivan et al. 2001), and by a factor of about 3 as their hosting group halo becomes more massive. EL and AGN galaxies define a far less clear picture; EL galaxies seem to occur at any M_B and $M_{\rm group}$ with a constant frequency, while their fraction decreases by a factor of about 1.5 as $M_{\rm dyn}$ gets larger. The percentage of AGN galaxies

drops by a factor of about 2 at brighter M_B values. It very weakly decreases in massive group halos, and appears quite insensitive to $M_{\rm dyn}$. As for the hierarchy inside a group, there is a weak indication that EL, FIRST and ROSAT galaxies are preferentially associated with central galaxies, while satellite galaxies are more frequently NA and AGN galaxies. Within the Poisson statistics, however, none of these trends with group hierarchy is significant.

4.2. The relation between activity and morphology

A first glance at how morphology varies with activity is provided by Table 2, which lists $f_{\rm disky}$ for the 5 classes defined in §4.1. As for Table 1, AGN, EL and NA galaxies are mutually exclusive, while any of them can be included in the FIRST and ROSAT categories. In this case, $f_{\rm disky}$ is derived from the pool of galaxies common to FIRST (ROSAT) and one of the optically active sub-samples. The ROSAT galaxies are clearly biased towards boxy shapes as their $f_{\rm disky}$ is systematically lower than ~ 0.50. AGN and NA galaxies with or without radio emission are generally disky (with $f_{\rm disky} > 0.60$). The radio emission seems to make a difference in the case of EL galaxies: while the full sub-sample of ELs is as disky as AGN and NA galaxies, those ELs detected by FIRST are dominated by boxy systems with $f_{\rm disky} \simeq 0.45$.

The upper panels of Figure 9 show scatter plots of the [OIII] luminosity, radio luminosity and X-ray luminosity as function of A_4. The lower panels plot the corresponding fractions of disky systems. In the lower left-hand panel, $f_{\rm disky}$ is plotted as function of L[OIII] for both AGN (filled squares) and EL (filled triangles) galaxies. This shows that both AGN and EL galaxies have a disky fraction that is consistent with that of the full H06 sample ($f_{\rm disky} = 0.66$), and with no significant dependence on the actual [OIII] luminosity. The grey lines (solid for AGN and dotted for EL galaxies) indicate the disky fractions predicted under the null-hypothesis that $f_{\rm disky}$ is a function only of M_B. These predictions are in excellent agreement with the data, suggesting that the (level of) optical activity does not help in better predicting the disky/boxy morphology of an early-type galaxy. The only possible exception is the sub-sample of EL galaxies with $\log(L_{\rm [OIII]}/L_\odot) < 5.2$ which has $f_{\rm disky} = 0.54$, approximately 3σ lower than given by the null-hypothesis.

The relatively small number of sample galaxies detected by FIRST and ROSAT prevents us from applying the above analysis as a function of radio and/or soft X-ray luminosity. Instead we have determined $f_{\rm disky}$ separately for the sub-samples of galaxies detected and not-detected by FIRST or ROSAT. The results are shown in the lower middle and lower right-hand panels of Figure 9. Clearly, the disky fraction of galaxies detected by ROSAT ($f_{\rm disky} = 0.48 \pm 0.08$) is significantly lower than those with no detected soft X-ray flux ($f_{\rm disky} = 0.66 \pm 0.02$), in agreement with the results of Bender et al. (1989) and Pellegrini (1999, 2005). The fact that galaxies detected by ROSAT are more boxy is expected since they are significantly brighter than those with no soft X-ray detection (cf. Figure 5). The grey lines, which correspond to $f_{\rm disky,0}(M_B)$, indicate that this explains most of the effect. Although it is intriguing that the disky fraction of ROSAT detections is $\sim 1\sigma$ lower than predicted, a larger sample of early-type galaxies with soft X-ray detections is

needed to rule out (or confirm) the null-hypothesis. As for the galaxies detected by FIRST, there is a weak indication that these galaxies have a somewhat lower $f_{\rm disky}$: this finding is again in excellent agreement with the predictions based on the null-hypothesis. Therefore, there is no indication that the morphology of an early-type galaxy is directly related to whether the galaxy is active in the radio or not.

To further test the null-hypothesis that the isophotal structure of early-type galaxies is entirely dictated by their absolute magnitude or dynamical mass, we have derived $f_{\rm disky}$ of NA, EL and AGN galaxies in bins of M_B and $M_{\rm dyn}$. The results are shown in Figure 10 (symbols), which shows that the disky fraction of all three samples decreases with increasing luminosity and dynamical mass. The grey solid and dashed lines indicate the predictions based on the null-hypothesis, which have been computed using equations (5)–(7). Overall, these predictions are in excellent agreement with the data, indicating that elliptical galaxies with ongoing star formation or with an AGN do not have a significantly different morphology (statistically speaking) than other ellipticals of the same luminosity or dynamical mass.

Finally, in Figure 11 we plot the disky fractions of NA, EL and AGN galaxies as function of their group mass (upper panels) and group hierarchy (lower panels). For comparison, the grey solid and dashed lines indicate the predictions based on the null-hypothesis. Although overall these predictions are in good agreement with the data, there are a few noteworthy trends. At the massive end ($M_{\rm group} \gtrsim 10^{13} h^{-1}\,{\rm M}_\odot$) the disky fraction of AGN is higher than expected, while that of NA galaxies is lower. The lower panels show that this mainly owes to the satellite galaxies in these massive groups. Whereas the null-hypothesis accurately predicts the disky fractions of NA, EL and AGN centrals, it overpredicts $f_{\rm disky}$ of NA satellites, while underpredicting that of AGN satellites at the 3 σ level. These results clearly warrant a more detailed investigation with larger samples. Note that only about half of the 847 galaxies in the H06 sample are also in our group catalog. A future analysis based on larger SDSS samples and a more complete group catalog would sufficiently boost the statistics to examine the trends identified here with higher confidence.

5. Discussion and conclusions

In spite of their outwardly bland and symmetrical morphology, early-type galaxies reveal a far more complex structure, whose isophotes usually deviate from a purely elliptical shape. As shown by Bender et al. (1989), these deviations correlate with other parameters; for example, boxy early-type galaxies are on average brighter and bigger than disky galaxies and are supported by anisotropic pressure. Early-type galaxies with disky isophotes, on the other hand, are consistent with being isotropic oblate rotators. With the advent of large galaxy redshift surveys such as the SDSS, it is now possible to collect large and homogeneous samples of early-type galaxies and quantify these correlations in much greater detail. In addition, it also allows for a detailed study of the relation between morphology and environment.

We have used a sample of 847 early-type galaxies imaged by the SDSS and analyzed by Hao et al. (2006a) to study the fraction of disky galaxies ($f_{\rm disky}$) as a function of their absolute magnitude M_B, their dynamical mass $M_{\rm dyn}$ and the mass of the dark matter halo $M_{\rm group}$ in which they are located. Using the Hα, Hβ, [OIII] and [NII] emission lines in the SDSS spectra we have split the sample in AGN galaxies, emission-line (EL) galaxies, and non-active (NA) galaxies (see Figure 4). In addition we also constructed two sub-samples of those ellipticals that have also been detected in the radio (in FIRST) or in soft X-rays (with ROSAT), and we have analyzed the relations between $f_{\rm disky}$ and the level of AGN activity in the optical and the radio, and the strength of soft X-ray emission.

The fraction of disky galaxies in the full sample decreases strongly with increasing luminosity and dynamical mass (see Figure 2). More quantitatively, $f_{\rm disky}$ decreases from ~ 0.8 at $M_B - 5\log(h) = -18.6$ ($M_{\rm dyn} = 6\times10^{10}h^{-1}M_\odot$) to ~ 0.5 at $M_B - 5\log(h) = -20.6$ ($M_{\rm dyn} = 3\times10^{11}h^{-1}M_\odot$). This indicates a smooth transition between disky and boxy shapes, which is well represented by a log-linear relation between $f_{\rm disky}$ and luminosity or dynamical mass (at least over the ranges probed here). The relatively large sample allows us to measure these relations with a good degree of accuracy that is robust against the uncertainties involved in the measurement of the A_4 parameter.

We have used these log-linear relations to test the null-hypothesis that the isophotal shape of early-type galaxies depends only on their absolute magnitude or dynamical mass. The main result of this paper is that the data is fully consistent with this simple ansatz, and that the correlations seen among group mass, group hierarchy (central *vs.* satellite), soft X-ray emission, activity (both in the optical and in the radio) and the disky/boxy morphology of an early-type galaxy reflect the dependence of each of these properties on galaxy luminosity. In fact, the luminosity (mass) dependence of $f_{\rm disky}$ predicts, with good accuracy, the following observed trends:

1. The variation of $f_{\rm disky}$ of central and satellite galaxies in the sample as a function of their group halo mass (see Figure 2).
2. The constancy of $f_{\rm disky}$ of EL and AGN galaxies with respect to their [OIII] luminosity (see Figure 9).
3. The decreasing $f_{\rm disky}$ of NA, EL and AGN galaxies with increasing M_B and $M_{\rm dyn}$ (see Figure 10).
4. The dependence of $f_{\rm disky}$ of NA, EL and AGN galaxies on their group halo mass and hierarchy (see Figure 11).
5. The average value of $f_{\rm disky}$ among those sample galaxies detected by ROSAT and FIRST.

The fact that our null-hypothesis is also consistent with the fraction of disky radio-emitters contradicts Bender et al. (1989), who wrote that "the isophotal shape is the second parameter besides

luminosity determining the occurance of radio activity in ellipticals". We claim instead, using a much larger, more homogeneous sample, that the radio activity is merely a reflection of the multivariate dependence of radio activity, luminosity and morphology. We have further checked this result using an inverse approach, based on the $f_{\rm radio}$ - M_B relation. Briefly, we derived, for the full sample, the fraction of radio galaxies ($f_{\rm radio}$) with respect to the total as a function of M_B, and obtained a log-linear relation whereby $f_{\rm radio}$ smoothly increases from 0.06 at $M_B - 5\log(h) = -18.7$ to 0.34 at $M_B - 5\log(h) = -20.7$. The fraction of radio galaxies among disky and boxy galaxies in the full sample turns out to be $f_{\rm radio}({\rm disky}) = 0.17 \pm 0.02$ and $f_{\rm radio}({\rm boxy}) = 0.23 \pm 0.02$. Entering the mean absolute magnitude of disky and boxy galaxies in the $f_{\rm radio}$ - M_B relation, we obtain radio fractions of 0.18 and 0.21, respectively, well within 1 σ from the observed values.

Although the data is in good overall agreement with the null-hypothesis, there are a few weak deviations at the 1 (3 at most) σ level (throughout errors have been computed assuming Poisson statistics). First of all, emission line galaxies with $\log(L_{\rm [OIII]}/L_\odot) < 5.2$ have a disky fraction that is $\sim 3\sigma$ lower than predicted by the null-hypothesis. Note however, that for higher [OIII] luminosities, the null-hypothesis is in excellent agreement with the disky fraction of EL galaxies. Another mild discrepancy between data and null-hypothesis regards the disky fraction of ellipticals detected by ROSAT, which is $\sim 1\sigma$ lower than predicted. Finally, the disky fraction of NA and AGN satellites in groups with $M_{\rm group} \gtrsim 10^{13} h^{-1}$ M$_\odot$ are slightly too high and low, with respect to the null-hypothesis, respectively. Whether these discrepancies indicate a true shortcoming of the null-hypothesis, and thus signal that the isophotal shape of early-type galaxies depends on additional parameters, requires a larger sample even. In the relatively near future, the final SDSS should be able to roughly double the size of the sample used here, while a group catalog of this final SDSS should increase the statistics regarding the environmental dependencies by an even larger amount.

The relations between $f_{\rm disky}$ and M_B ($M_{\rm dyn}$) derived here provide a powerful test-bench for theories of galaxy formation. In particular, they can be used to constrain the nature and the merging history of the progenitors of present-day early-type galaxies. In a follow-up paper, we will use semi-analytical models featuring AGN and supernova feedback in order to predict and understand the observed log-linear relations in terms of the amount of cold gas in the progenitors at the time of the last merger and their mass ratio (Kang et al., in prep).

AP acknowledges useful discussions with Sandra Faber and John Kormendy. We thank an anonymous referee for his/her useful comments on the paper. Funding for the creation and distribution of the SDSS Archive has been provided by the Alfred P. Sloan Foundation, the Participating Institutions, the National Aeronautics and Space Administration, the National Science Foundation, the U.S. Department of Energy, the Japanese Monbukagakusho, and the Max Planck Society. The SDSS Web site is http://www.sdss.org/. The SDSS is managed by the Astrophysical Research Consortium (ARC) for the Participating Institutions. The Participating Institutions are The Uni-

versity of Chicago, Fermilab, the Institute for Advanced Study, the Japan Participation Group, The Johns Hopkins University, the Korean Scientist Group, Los Alamos National Laboratory, the Max-Planck-Institute for Astronomy (MPIA), the Max-Planck-Institute for Astrophysics (MPA), New Mexico State University, University of Pittsburgh, University of Portsmouth, Princeton University, the United States Naval Observatory, and the University of Washington.

REFERENCES

Adelman-McCarthy, J.K., et al. 2006, ApJS, 162, 38

Anderson, S.F., et al. 2003, AJ, 126, 2209

Baldwin, J., Phillips, M., Terlevich, R. 1981, PASP, 93, 5

Barnes, J.E., Hernquist, L.E. 1991, ApJL, 370, L65

Barnes, J.E., Hernquist, L.E. 1996, ApJ, 471, 115

Becker, R.H., White, R.L., Helfand, D.J. 1995, ApJ, 450, 559

Bender, R. 1988, A&AS, 193, 7

Bender, R., Döbereiner, S., Möllenhoff, C., 1988, A&AS, 74, 385

Bender, R., Möllenhoff, C. 1987, A&A, 177, 71

Bender, R., Surma, P., Döbereiner, S., Mo̊llenhoff, C., Madejsky, R. 1989, A&A, 217, 35

Bernardi, M., et al. 2003, AJ, 125, 1817

Best, P.N., Kauffmann, G., Heckman, T.M., Brinchmann, J., Charlot, S., Ivezić, Z., White, S.D.M. 2005, MNRAS, 362, 25

Blanton, M.R., et al. 2005, AJ, 129, 2562

Bower, R.G., Lucey, J.R., Ellis, R.S. 1992, MNRAS, 254, 601

Canizares, C.R., Fabbiano, G., Trinchieri, G. 1987, ApJ, 312, 503

Cappellari, M., et al. 2006, MNRAS, 366, 1126

Carter, D. 1987, ApJ, 312, 514

Cattaneo, A., Blaizot, J., Devriendt, J., Guiderdoni, B. 2005, MNRAS, 364, 407

Croton, D.J., et al. 2005, MNRAS, 356, 1155

Djorgovski, S., Davis, M. 1987, ApJ, 313, 59

Davies, R.L., Efstathiou, G., Fall, S.M., Illingworth, G., Schechter, P.L. 1983, ApJ, 266, 41

Dressler, A. 1980, ApJ, 236, 351

Dressler, A. 1987, ApJ, 317, 1

Ellis, R.S., Smail, I., Dressler, A., Couch, W.J., Oemler, A.Jr., Butcher, H., Sharples, R.M. 1997, ApJ, 483, 582

Fabbiano, G. 1989, ARA&A, 27, 87

Faber, S.M., Jackson, R.E. 1976, ApJ, 204, 668

Faber, S.M., et al. 1997, AJ, 114, 1771

Ferrarese, L., van den Bosch, F.C., Ford, H.C., Jaffe, W., O'Connell, R.W. 1994, AJ, 108, 1598

Gebhardt, K., et al. 1996, AJ, 112, 105

Graham, A.W., Erwin, P, Caon, N., Trujillo, I. 2001, ApJ, 563, L11

Hao, C.N., Mao, S., Deng, Z.G., Xia, X.Y., Wu, H. 2006a, MNRAS, 370, 1339

Hao, C.N., Mao, S., Deng, Z.G., Xia, X.Y., Wu, H. 2006b, MNRAS, 373, 1264

Jaffe, W., Ford, H.C., O'Connell, R.W., van den Bosch, F.C., Ferrarese, L. 1994, AJ, 108, 1567

Jedrzejewski, R.I. 1987, MNRAS, 226, 747

Jesseit, R., Naab, Y., Burkert, A. 2005, MNRAS, 360, 1185

Kang, X., van den Bosch, F.C., Pasquali, A., 2007, preprint (arXiv:0704.0932)

Kauffmann, G., et al. 2003a, MNRAS, 341, 33

Kauffmann, G., et al. 2003b, MNRAS, 346, 1055

Kewley, L.J., Groves, B., Kauffmann, G., Heckman, T., 2006, MNRAS, 372, 961

Khochfar, S., Burkert, A. 2005, MNRAS, 359, 1379

Kuntschner, H., et al. 2006, MNRAS, 369, 497

Lauer, T.R. 1985, MNRAS, 216, 429

Lauer, T.R., et al. 1995, AJ, 110, 2622

Lauer, T.R., et al. 2005, AJ, 129, 2138

McMahon, R.G., White, R.L., Helfand, D.J., Becker, R.H. 2002, ApJ Supl.Ser., 143, 1

Mihos, J.C., Hernquist, L.E. 1994, ApJL, 425, L13

Mihos, J.C., Hernquist, L.E. 1996, ApJ, 464, 641

Milosavljević, M., Merritt D., Rest A., van den Bosch F.C. 2002, MNRAS, 331, 51

Morganti, R., et al. 2006, MNRAS, 371, 157

Naab, Y., Jesseit, R., Burkert, A. 2006, MNRAS, in press (astro-ph/0605155)

Nieto, J.-L., Capaccioli, M., Held, E.V. 1988, A&A, 195, 1

O'Sullivan, E., Forbes, D.A., Ponman, T.J. 2001, MNRAS, 328, 461

Pellegrini, S. 1999, A&A, 351, 487

Pellegrini, S. 2005, MNRAS, 364, 169

Ravindranath, S., Ho, L.C., Peng, C.Y., Filippenko, A.V., Sargent, W.L.W. 2001, AJ, 122, 653

Rest, A., et al. 2001, AJ, 121, 2431

Sarzi, M., et al. 2006, MNRAS, 366, 1151

Scorza, C., Bender, R. 1995, A&A, 293, 20

Scorza, C., van den Bosch, F.C. 1998, MNRAS, 300, 469

Serra, P., Trager, S.C., van der Hulst, J.M., Oosterloo, T.A., Morganti, R. 2006, A&A, 453, 493

Shioya, Y., Taniguchi, Y. 1993, PASJ, 43, 39

Smith, J.A. et al. 2002, AJ, 123, 2121

Springel, V. 2000, MNRAS, 312, 859

Stoughton, C., et al., 2002, AJ, 123, 485

Strauss, M.A., et al, 2002, AJ, 124, 1810

Toomre, A., Toomre, J. 1972, ApJ, 178, 623

Trager, S.C., Faber, S.M., Worthey, G., González, J.J. 2000, AJ, 119, 1645

Tran, H.D., Tsvetanov, Z., Ford, H.C., Davies, J., Jaffe, W., van den Bosch, F.C., Rest, A. 2001, AJ, 121, 2928

Trinchieri, G., Fabbiano, G. 1985, ApJ, 296, 447

Veilleux, S., Osterbrock, D. 1987, ApJS, 63, 295

Visvanathan, N., Sandage, A. 1977, 216, 214

Voges, W., et al. 1999, A&A, 349, 389

Weinmann, S., van den Bosch, F.C., Yang, X., Mo, H.J. 2006, MNRAS, 366, 2

Yang, X., Mo, H.J., van den Bosch, F.C., Jing, Y.P. 2005, MNRAS, 356, 1293

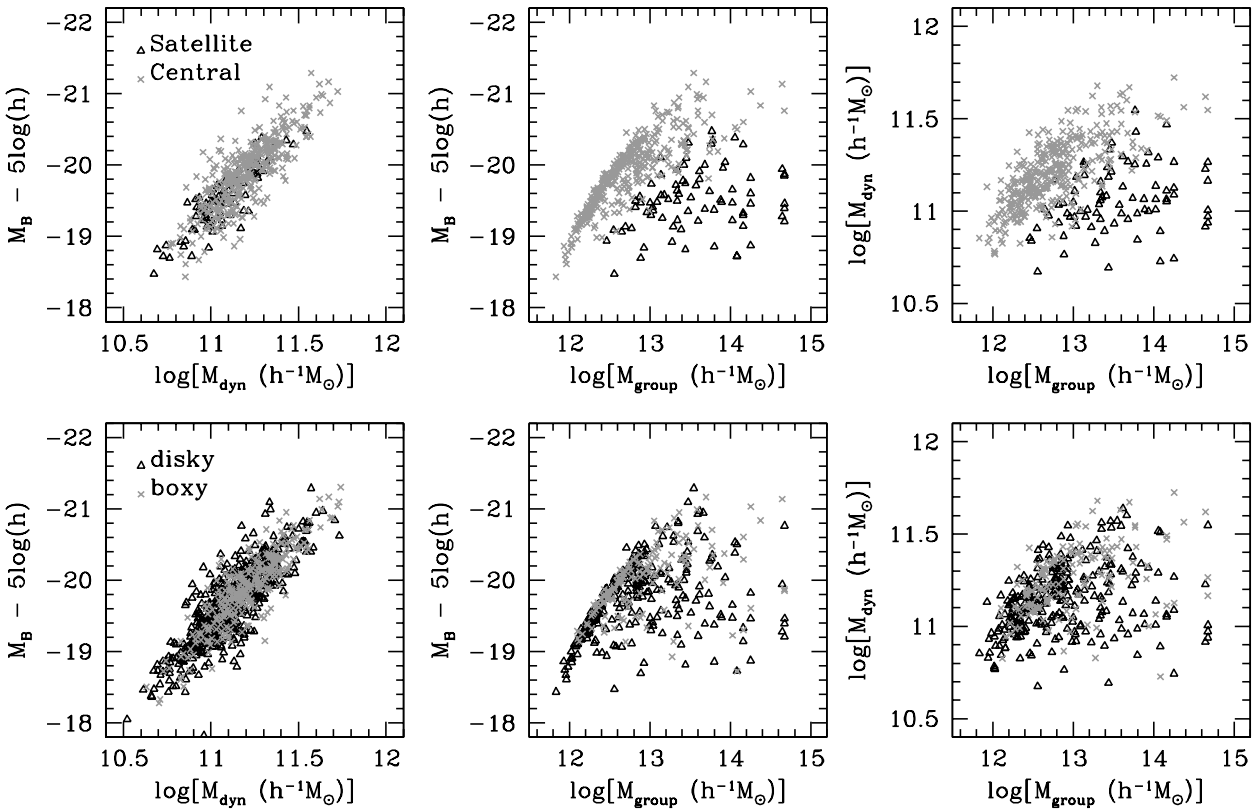

Fig. 1.— The distributions in M_B, $M_{\rm dyn}$ and $M_{\rm group}$ for the full sample, split between central and satellite galaxies (grey crosses and open triangles respectively, in the top panels) and between disky and boxy galaxies (open triangles and grey crosses respectively, in the bottom panels).

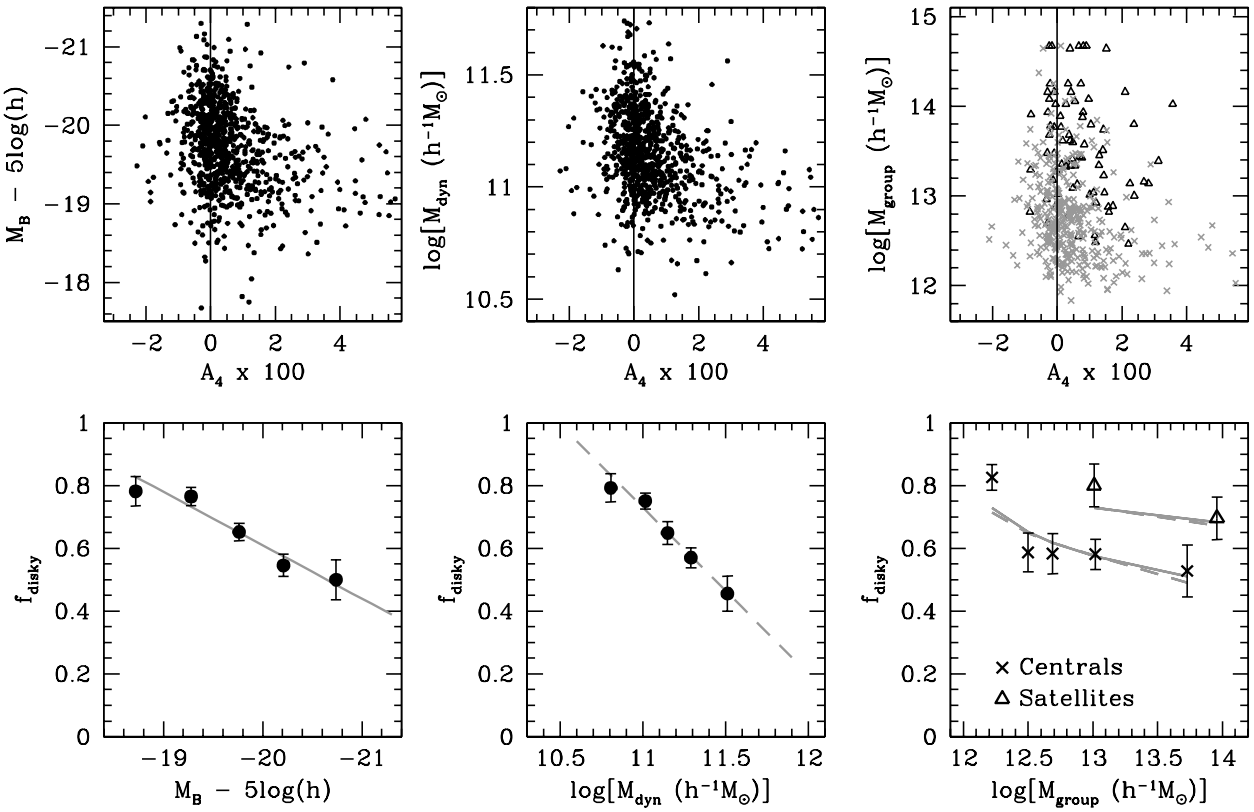

Fig. 2.— *Top panels:* the distributions of M_B, $M_{\rm dyn}$ and $M_{\rm group}$ as a function of the isophotal parameter A_4 for the full sample, also split between central (grey crosses) and satellite (open triangles) galaxies. *Bottom panels:* the fraction of disky galaxies as a function of M_B and $M_{\rm dyn}$ for the full sample. The fraction of disky galaxies is also shown per bin of group halo mass $M_{\rm group}$ for central (crosses) and satellite (open triangles) galaxies. The errorbars are at the 1 σ level, and were computed assuming Poisson statistics. The grey solid and dashed lines in the left hand-side and middle panels are the best fits to the fractions of disky galaxies across the full sample. The same lines in the right hand-side panel represent the predicted fractions of disky galaxies from the working null-hypothesis.

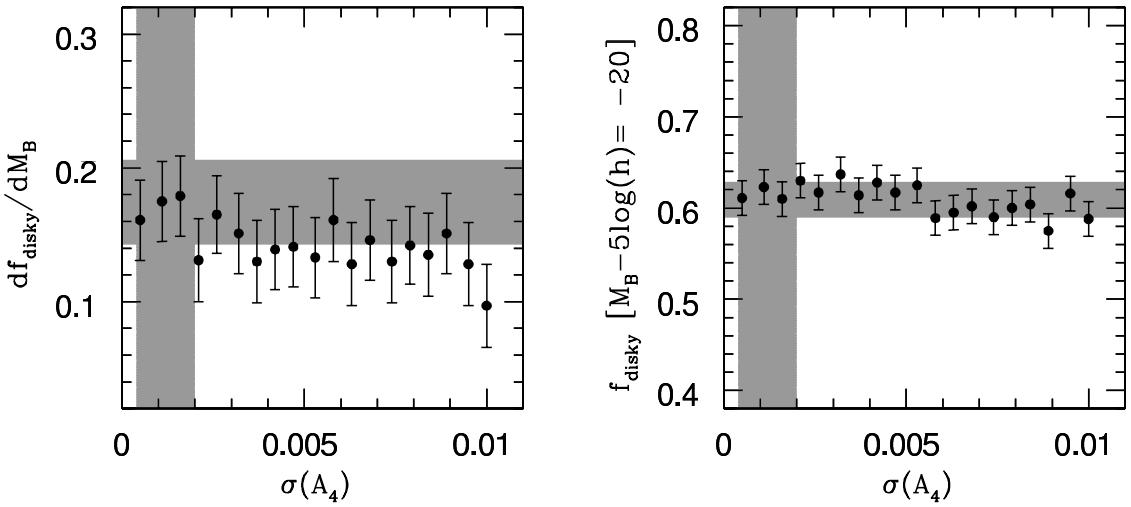

Fig. 3.— Impact of individual A_4 measurement errors: the slope and the zero-point of the log-linear correlation between $f_{\rm disky}$ and M_B (equation 4) are shown as a function of the standard deviation of the Gaussian used to simulate errors on the observed A_4 values. The grey shaded areas indicate the best-fitting slope (0.17 ± 0.03) and zero-point (0.61 ± 0.02) in equation 4, and the mean uncertainty on the observed A_4 parameter (0.0012 ± 0.0008) as measured by H06.

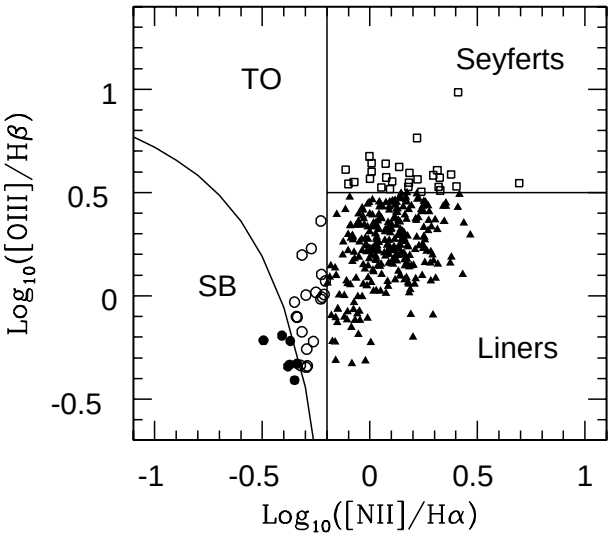

Fig. 4.— The BPT diagram for the galaxies in the full sample, whose [OIII] λ5007 and Hα emission lines were detected with a S/N ratio larger than 3. These objects have been split among Seyfert galaxies of type 2, LINERs, Transition Objects (TO) and star-forming (SB) according to Kauffmann et al. (2003b).

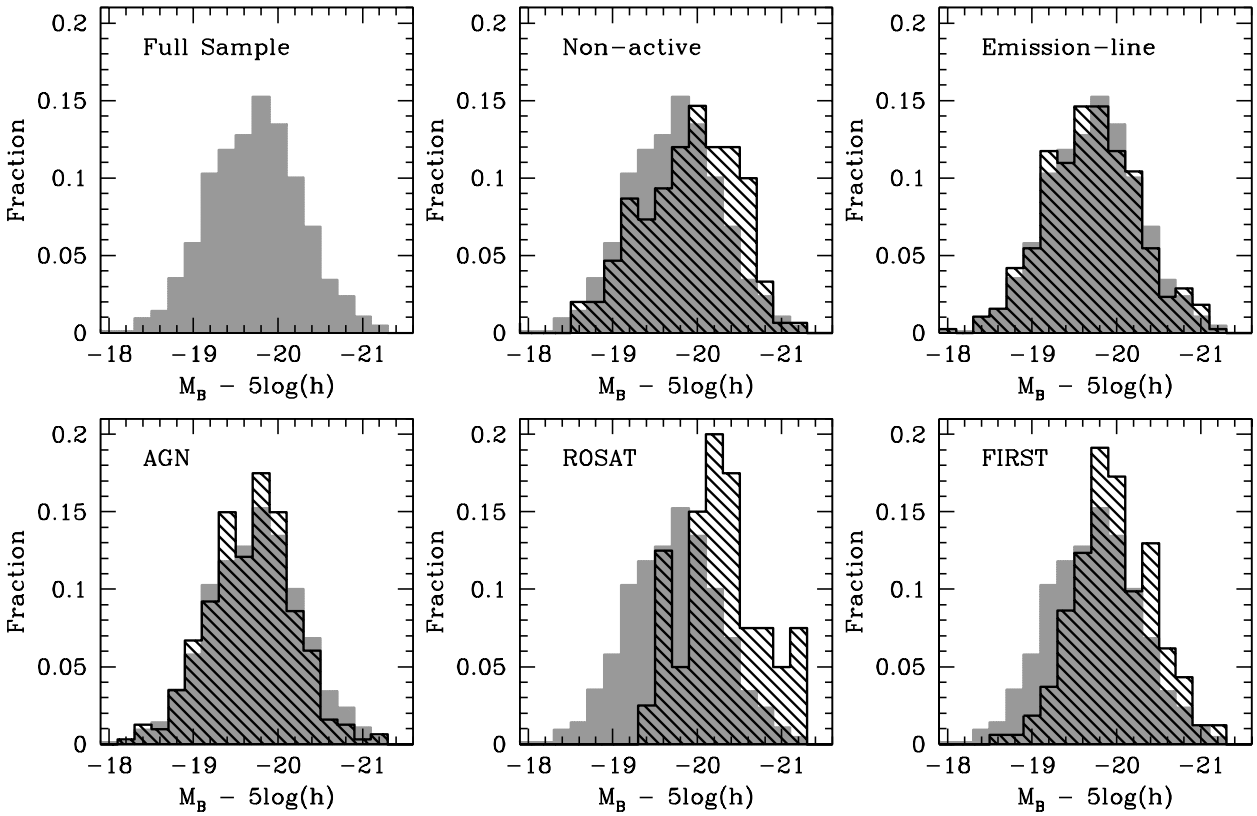

Fig. 5.— The distributions of the full sample (grey shaded area) and the 5 different activity classes defined in §4.1 in absolute magnitude M_B (in AB system). Each distribution is normalized by the size of the sample from where it was extracted.

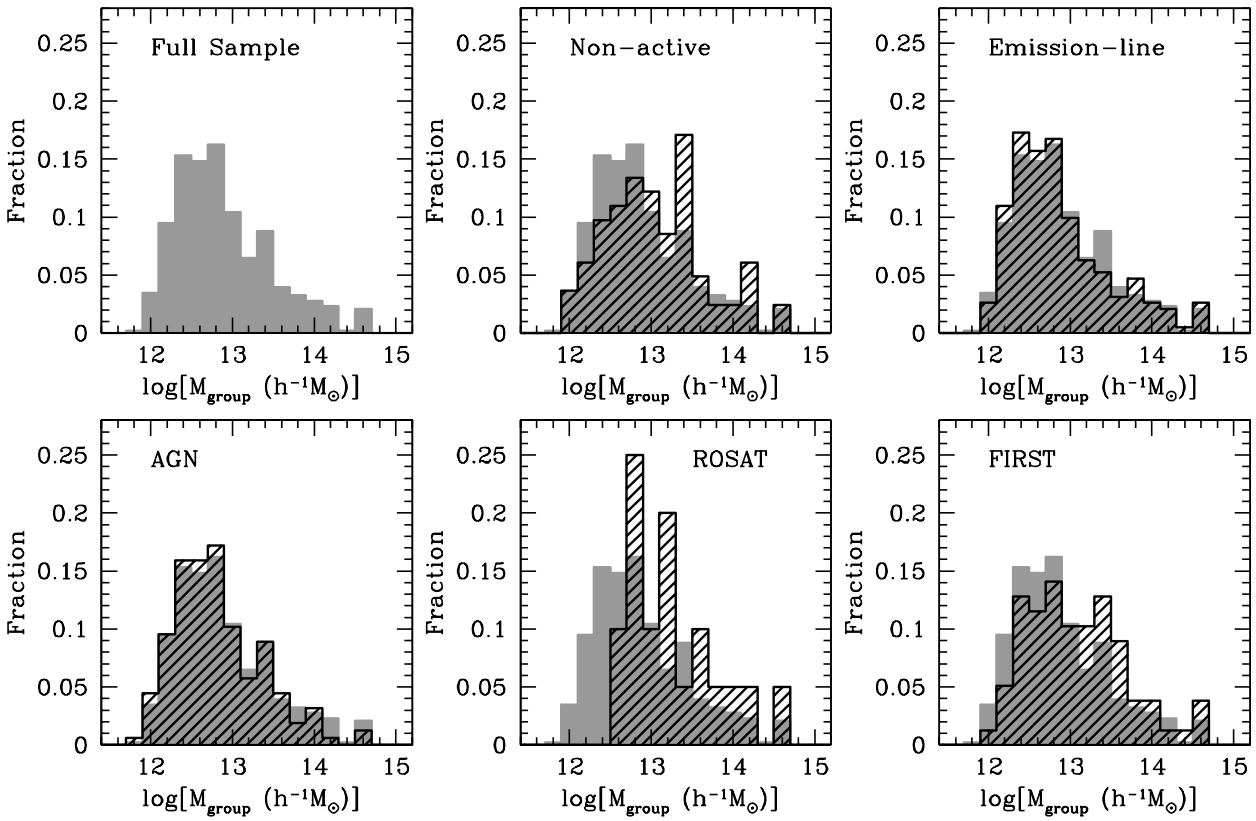

Fig. 6.— As in Figure 5, but for the group halo mass $M_{\rm group}$.

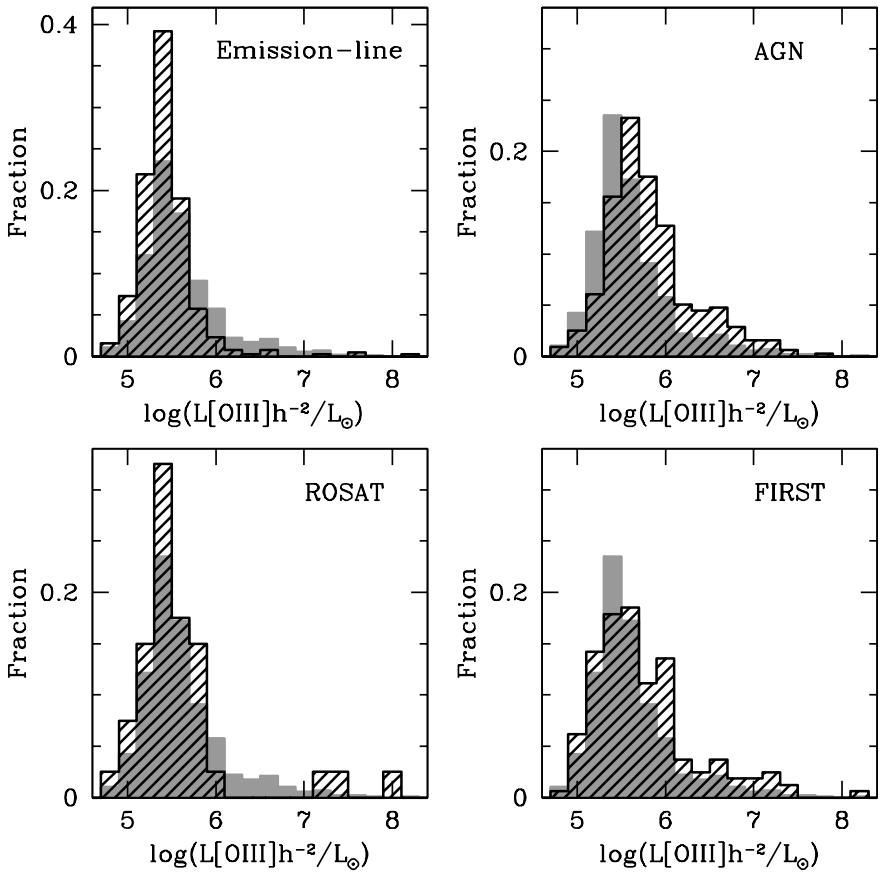

Fig. 7.— As in Figure 5, but for the luminosity in the [OIII] line. Here, the grey shaded histogram refers to emission-line and AGN galaxies together.

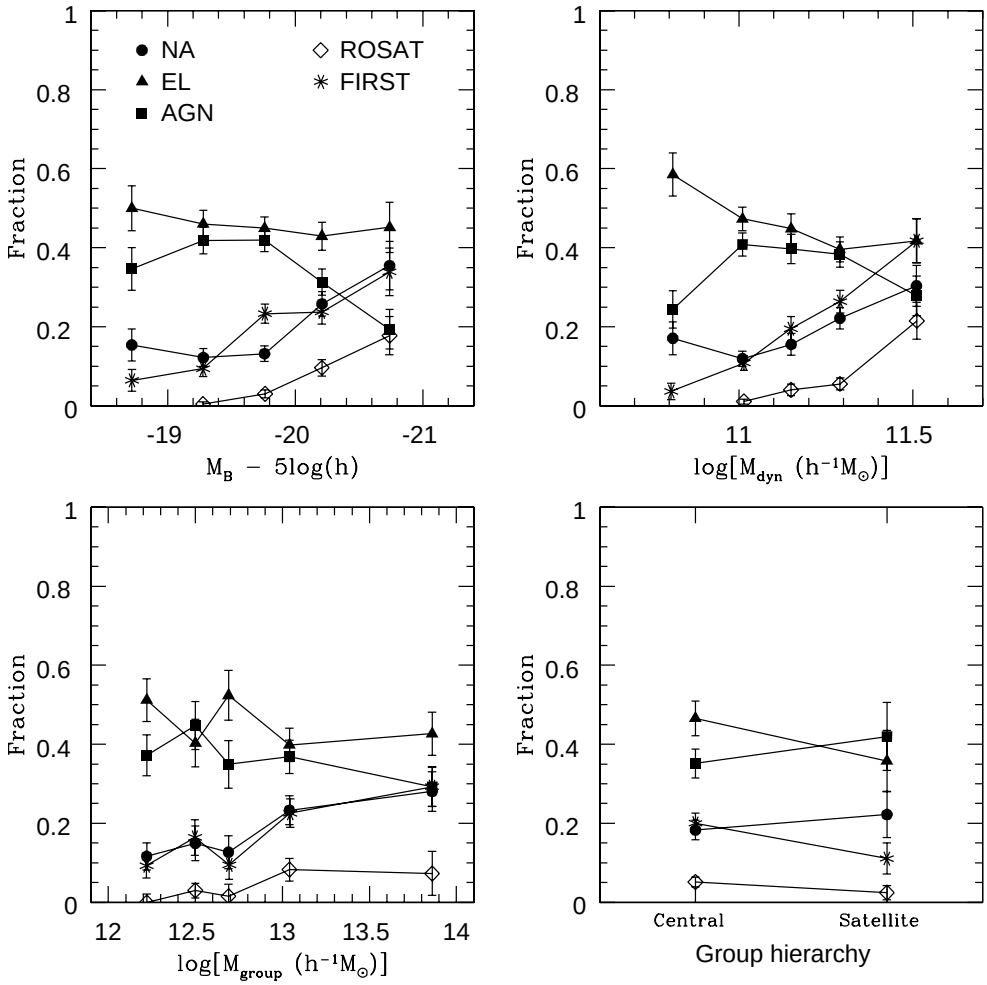

Fig. 8.— The fraction of galaxies in the 5 different activity classes with respect to the full sample as a function of M_B, $M_{\rm dyn}$, $M_{\rm group}$ and split between centrals and satellites.

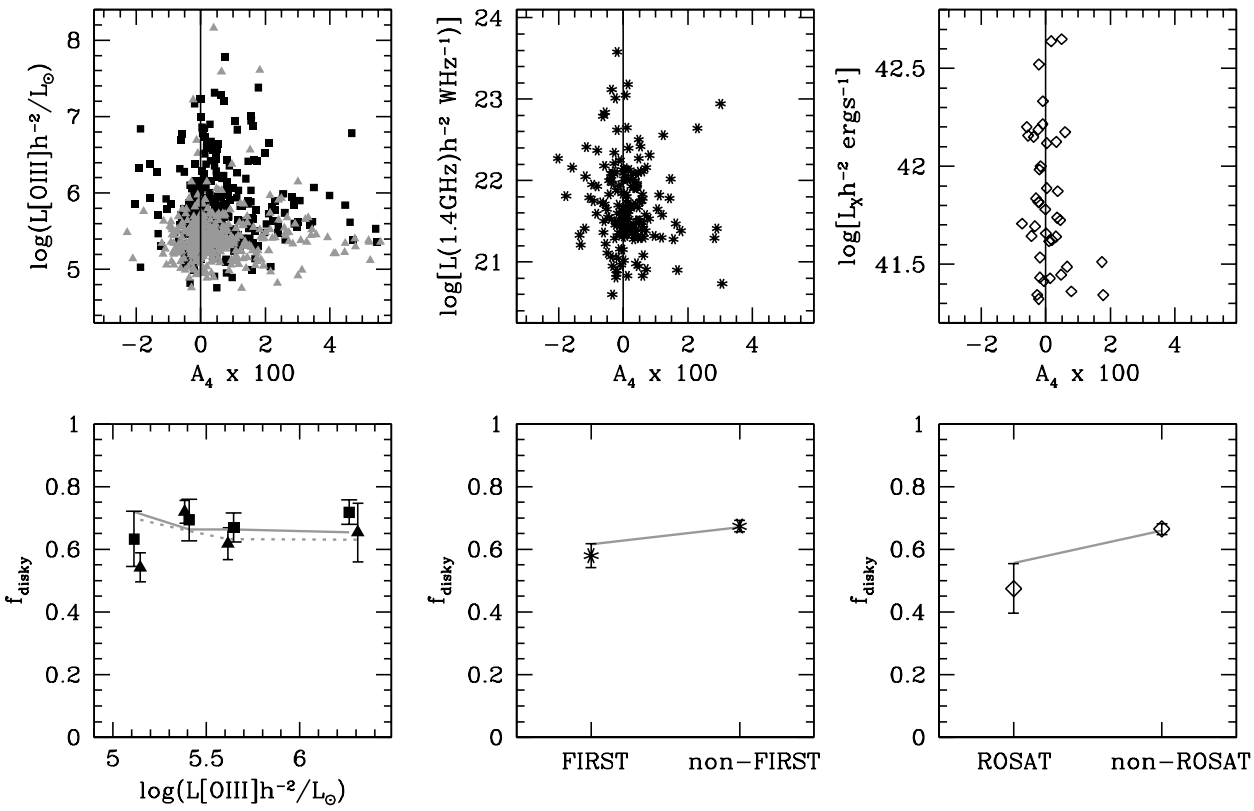

Fig. 9.— *Top panels:* the distribution of the luminosities in the [OIII] line, at 1.4 GHz and in the soft X-rays, as a function of the isophotal parameter A_4. Emission-line and AGN galaxies are represented with grey filled triangles and black filled squares respectively. *Bottom panels:* the fraction of disky galaxies among emission-line (triangles) and AGN (squares) galaxies as a function of the luminosity in the [OIII] line (left hand-side panel). The grey solid and dotted lines trace the predictions from the working null-hypothesis in M_B. The fraction of disky galaxies for the galaxies detected and non-detected by FIRST and ROSAT are shown in the middle and right hand-side panels, together with the predictions from equations (4) and (5). The errorbars are at the 1 σ level, and were computed assuming Poisson statistics.

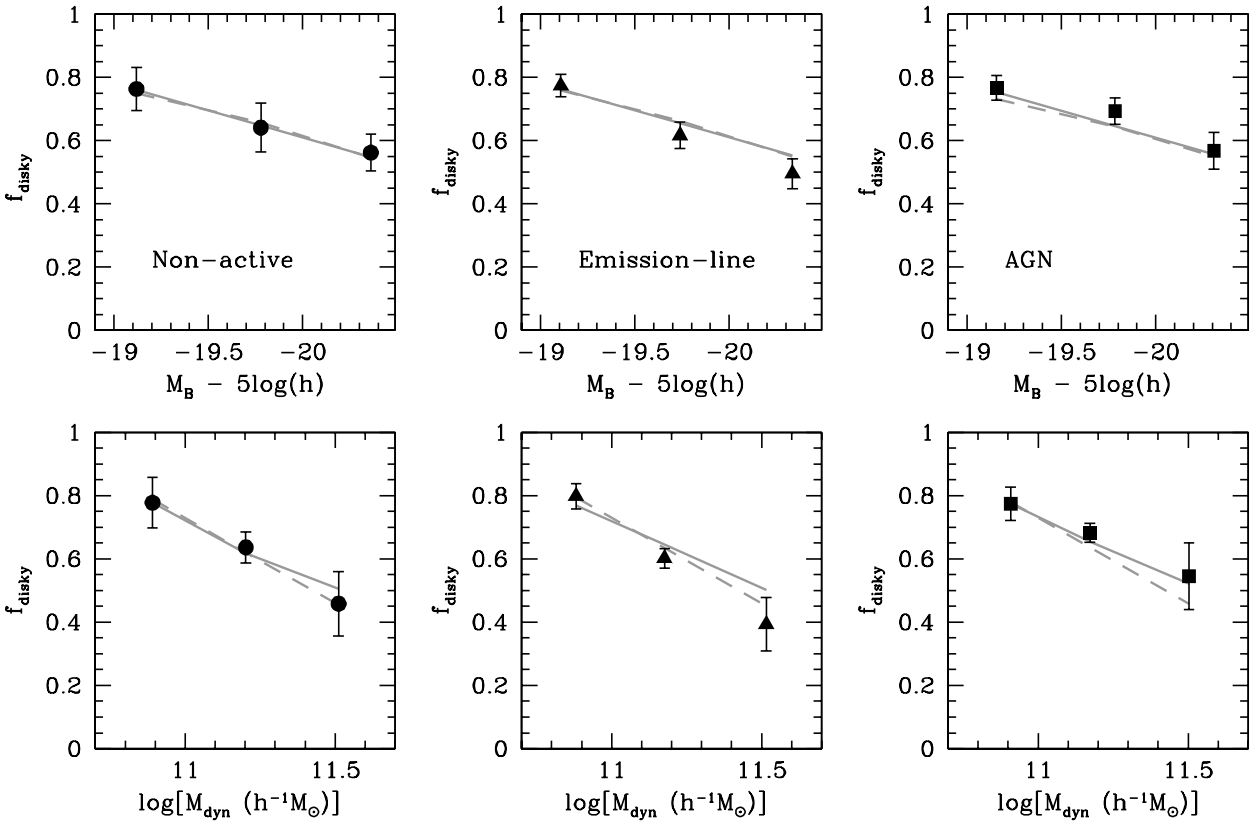

Fig. 10.— The fraction of disky galaxies for non-active (black filled circles), emission-line (black filled triangles) and AGN (black filled squares) galaxies as a function of M_B and $M_{\rm dyn}$. The grey solid and dashed lines represent the predictions from equation (5), i.e. the working null-hypothesis. The errorbars are at the 1 σ level, and were computed assuming a Poisson statistics.

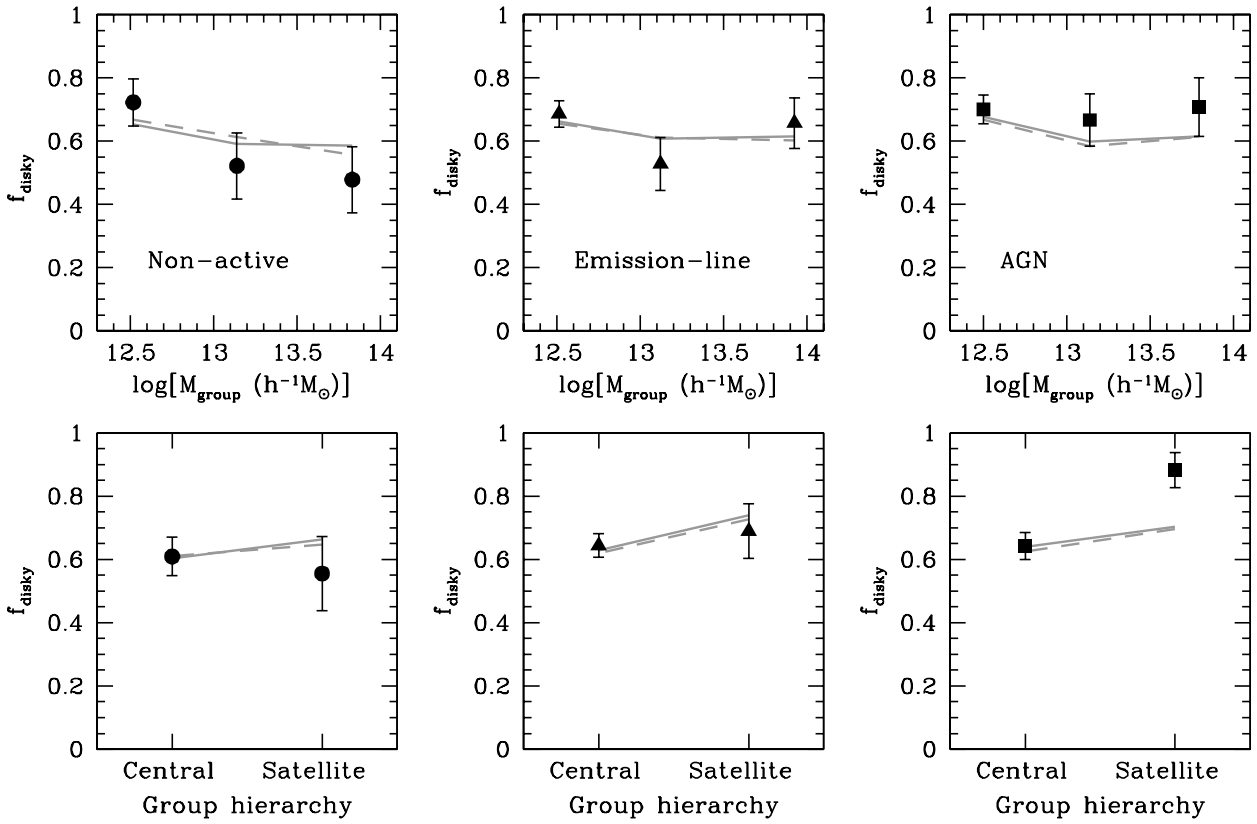

Fig. 11.— As in Figure 10, but splitting the non-active, emission-line and AGN galaxies between centrals and satellites.

Table 1. Activity Classes

	AGN	EL	NA	FIRST	ROSAT
AGN	314	−−	−−	91	17
EL	−−	383	−−	53	16
NA	−−	−−	150	18	7
FIRST	91	53	18	162	22
ROSAT	17	16	7	22	40

Note. — The number of sample galaxies in the five different activity classes. Note that the AGN, EL and NA classes are mutually exclusive.

Table 2. Fraction of disky galaxies across the activity classes

	AGN	EL	NA	FIRST	ROSAT
AGN	0.69	−−	−−	0.65	0.47
EL	−−	0.64	−−	0.45	0.50
NA	−−	−−	0.63	0.61	0.43
FIRST	0.65	0.45	0.61	0.58	0.54
ROSAT	0.47	0.50	0.43	0.54	0.47